Applied Biochemistry and Biotechnology
https://doi.org/10.1007/s12010-023-04676-7

ORIGINAL ARTICLE

Engineering of Methionine Adenosyltransferase Reveals Key Roles of Electrostatic Interactions in Enhanced Catalytic Activity

Weibin Lin[1] · Qiangqiang Wang[1] · Ruizhi Han[1] · Jinghui Zhou[2] · Gang Xu[2] · Ye Ni[1]

Accepted: 16 August 2023

Abstract
As an important dietary supplement, S-adenosylmethionine (SAM) is currently synthesized by methionine adenosyltransferase (MAT) using ATP and methionine as substrates. However, the activity of MAT is severely inhibited by product inhibition, which limits the industrial production of SAM. Here, MAT from *Bacteroides fragilis* (*Bf*MAT), exhibiting relatively low product inhibition and moderate specific activity, was identified by gene mining. Based on molecular docking, residues within 5 Å of ATP in *Bf*MAT were subjected to mutagenesis for enhanced catalytic activity. Triple variants M3-1 (E42M/E55L/K290I), M3-2 (E42R/E55L/K290I), and M3-3 (E42C/E55L/K290I) with specific activities of 1.83, 1.81, and 1.94 U/mg were obtained, which were 110.5–125.6% higher than that of the wild type (WT). Furthermore, compared with WT, the K_m values of M3-1 and M3-3 were decreased by 31.4% and 60.6%, leading to significant improvement in catalytic efficiency (k_{cat}/K_m) by 322.5% and 681.1%. All triple variants showed shifted optimal pH from 8.0 to 7.5. Moreover, interaction analysis suggests that the enhanced catalytic efficiency may be attributed to the decreased electrostatic interactions between ATP and the mutation sites (E42, E55, and K290). Based on MD simulation, coulomb energy and binding free energy analysis further reveal the importance of electrostatic interactions for catalytic activity of *Bf*MAT, which could be an efficient strategy for improving catalytic performance of MATs.

Keywords Methionine adenosyltransferase · Electrostatic interaction · Semi-rational engineering · Molecular dynamics simulation · Catalytic activity

✉ Ruizhi Han
hanrz@jiangnan.edu.cn

✉ Ye Ni
yni@jiangnan.edu.cn

[1] Key Laboratory of Industrial Biotechnology, Ministry of Education, School of Biotechnology, Jiangnan University, Wuxi 214122, China

[2] National Engineering Research Center for Enzyme Technology in Medicine and Chemical Industry, Hunan Flag Bio-Tech Co., Ltd., Changsha 410100, China

Published online: 29 August 2023

Introduction

S-adenosylmethionine (SAM) is an important physiologically active substance, existing in animals, plants, and microorganisms, and participating in a variety of biochemical reactions [1, 2]. As a precursor of three metabolic pathways (e.g., methyl, thio, and aminopropyl transfer reactions), SAM is generally recognized as a key intracellular methyl donor to various acceptors [3]. It can also be used for the treatment of liver health and injury [4], depression [5], arthritis [6], and so on. Besides, it is a potential candidate for morphine tolerance due to its documented safety in chronic use [7]. Microbial fermentation is commonly performed for SAM production from methionine, and extensive studies have been carried out to improve SAM production by metabolic engineering [8]. *Saccharomyces cerevisiae* and *Pichia pastor* are usually employed as model strains to produce SAM [9]. For instance, SAM yield was increased to 1.2 g/L (20 times of the parental strain) after overexpression *mat* in *P. pastoris* [10]. By adding aristeromycin and ethanol to suppress SAM consumption, SAM levels of 11.83 g/L were accumulated by P_{AOX}-*Pichia* after 65 h [11]. To reduce fermentation cost, $_{D}$-amino acid oxidase from *Trigonopsis variabilis* and $_{L}$-phenylalanine dehydrogenase from *Rhodococcus jostii* were introduced into *S. cerevisiae* to synthesize $_{L}$-methionine from $_{D}$-methionine, and a high SAM yield of 10.3 g/L was accumulated at 80 h by feeding 16 g/L $_{DL}$-methionine [12]. In the above reports, enhanced SAM production has been achieved by fermentation; however, some major deficiencies still exist, such as long fermentation time and difficult product recovery [13].

Biocatalytic production of SAM using methionine adenosyltransferase (MAT, EC 2.5.1.6) is an alternative approach due to its simple and efficient process, as well as easy product purification. However, MATs from most microorganisms exhibit severe product inhibition, which is undesirable for the industrial production of SAM [13]. Several protein engineering approaches have also been reported to reduce the product inhibition of MAT. For instance, product inhibition of MAT from *Escherichia coli* was reduced through decreasing the hydrogen bond interactions between SAM and residues Q99 and I103 [14]. MAT from *Campylobacter jejuni* was found with good tolerance toward a range of ester derivatives, especially for N, N-dimethyl-L-methionine methyl ester and SAM [2]. To reduce the product inhibition of MAT from *Bacillus subtilis*, the substitution of isoleucine by valine at site 317 was performed to shorten the distance between the methyl group of SAM and residue 317 [15]. However, product inhibition is still a major issue for SAM production by MATs from most microorganisms. In addition, the low activity of MATs is also a serious problem for enzymatic production of SAM. Multiple sequence alignment and structural analysis have also been employed to enhance the MAT activity. For example, variant I303V/I65V/L186V/N104K from *E. coli* was constructed with 3-time enhanced activity compared with WT [14].

Electrostatic interaction is often considered as a main impact factor for the regulation of substrate binding, catalytic conformation, and activity of enzymes. For instance, the positively charged surface with suitable surface charge density has been reported to be beneficial for haloalkane decomposition reaction catalyzed by haloalkane dehalogenase [16]. Changes in charge distribution could greatly affect the substrate binding. In this study, MAT from *Bacteroides fragilis* (*Bf*MAT) was employed for SAM production due to its relatively lower product inhibition than other MATs. However, SAM yield was limited by its low specific activity. Herein, saturation and combinatorial mutagenesis of residues lining the substrate-binding pocket were performed to enhance the catalytic

performance of *Bf*MAT. Furthermore, based on molecular dynamic simulation, mechanisms of enhanced activity and catalytic efficiency were elucidated.

Material and Methods

Bacterial Strain, Plasmid, and Reagents

Strains *E. coli* BL21(DE3), *E. coli* DH5α, and plasmid pET28a(+) were preserved in our laboratory. The genomic DNA was extracted from *E. coli* BL21(DE3) using bacterial genomic DNA extraction kit. *E. coli* DH5α was used to preserve plasmids. *E. coli* BL21(DE3) was used to express recombinant MATs. All the reagents of biochemical grade were obtained from domestic companies.

Construction of Recombinant Strain

MAT encoding gene from *E. coli* was amplified by 2 × Phanta Max Master Mix with the following primers: 5′- cagcaaatgggtcgcggatccATGGCAAAACACCTTTTTACGTC-3′ (forward primer) and 5′- tgcggccgcaagcttgtcgacTTACTTCAGACCGGCAGCATC-3′ (reverse primer), which contain restriction endonuclease sites of *Bam* HI and *Xho* I (underlined) and homologous fragments to vector pET28a(+). MAT encoding genes from *Campylobacter jejuni* (VTX77142.1), *Cryptosporidium parvum* (XP_628436.1), *Thermococcus kodakarensis* (WP_011249500.1), and *Bacteroides fragilis* (WP_005783643.1) were cloned in the pET28a(+) by the Tianlin Biotechnology (Wuxi, China). Vector pET28a(+) was double digested by restriction endonucleases *Bam*H I and *Xho* I, and the consequent segments were purified by Gel Purification Kits. After cloned with Seamless Cloning Kits, the recombinant plasmid pET28a-MAT was transformed into *E. coli* to obtain recombinant strain *E. coli* BL21(DE3)/pET28a-MAT.

Expression and Purification of MATs

The recombinant strain *E. coli* BL21(DE3)/pET28a-MAT was cultivated in LB medium containing 50 μg/mL kanamycin at 37 ℃, with 180 rpm shaking overnight, then inoculated into 40 mL fresh LB medium containing 50 μg/mL kanamycin. When the OD_{600} reached 0.6–0.8, the recombinant strain was induced with 0.2 mM isopropyl-β-D-thiogalactopyranoside (IPTG) and cultivated at 25 ℃, with shaking at 180 rpm for 12 h. Cells were harvested by centrifugation at 8000 × g for 5 min at 4 °C. After washing with 100 mM Tris–HCl buffer (pH 8.0), the cell pellets were re-suspended in the same buffer, then ultrasonicated at 300 W for 10 min to obtain crude enzyme solution. After centrifugation, the crude enzyme solution was purified by Ni–NTA affinity column. Purified MAT was verified by SDS-PAGE and stored at − 80 ℃.

High-Throughput Screening Method of MATs

The high-throughput screening method was established according to the literature [17]. Phosphate produced by the MAT can form a blue substance with ammonium molybdate in an acidic environment and has a characteristic absorption peak at 655 nm. The assay was

performed in 96-well plates. Three MATs and the variants were cultivated in 96-well plate containing 300 μL LB medium with 50 mg/L kanamycin in each well at 37 ℃ 180 rpm for 8 h. Culture (50 μL) mentioned above was withdrawn into another 96-well plate containing 600 μL LB medium with 50 mg/L kanamycin, then cultivated at 37 ℃ 180 rpm for 2 h. After cultivation, IPTG was added to each well to a final concentration of 1.4 mM, then the plate was cultivated at 25 ℃ 180 rpm for 12 h. The plate was centrifuged at 8000 × g for 5 min at 4 °C, the cells were re-suspended with 400 μL 750 mg/L lysozyme dissolved in 100 mM Tris–HCl buffer (pH 8.0), then incubated at 37 ℃ 180 rpm for 1 h to obtain cell lysates.

For activity assay, 19 μL cell lysate was mixed with 6 μL substrate solution (100 mM KCl, 20 mM $MgCl_2$, 2 mM ATP, and 10 mM methionine in 100 mM Tris–HCl buffer, pH 8.0). After incubation at 37 °C for 10 min, 25 μL ammonium moly bate (1% w/v $(NH_4)_6Mo_7O_{24}{\cdot}4H_2O$ in ddH_2O) and 50 μL L-ascorbic acid (12% w/v L-ascorbic acid in 1 M HCl) were added. Following incubation at room temperature for 5 min, a solution containing 2% w/v acetic acid and 2% sodium citrate tribasic dihydrate in ddH_2O was added. The reaction was incubated at room temperature for 15 min. The concentration of phosphate was determined at 655 nm in a microplate reader (BioTek PowerWave XS2). Variants that showed a deeper blue than their wild type were isolated for another round of screening. The product inhibition of MAT was determined by the method mentioned above with additional SAM of different concentrations.

Saturation Mutagenesis of BfMAT

Primers were designed by CE designer (Table S1). PCR mixture contained 0.5 μL template (50 ng/μL), 1 μL forward primer, 1 μL reverse primer, 12.5 μL 2 × Phanta Max Master Mix, and 10 μL ddH_2O. The PCR amplification procedure included pre-denaturation at 95 ℃ for 30 s, 95 °C for 15 s, 55 °C for 15 s, 72 °C for 360 s (25 cycles), and complete extension at 72 °C for 5 min. The PCR template was digested with *Dpn* I. The digested products were transformed into 100 μL competent cells. Cells were cultivated in 800 μL LB medium at 37 °C for 1 h, then 100 μL cells were spread on LB solid plate and cultured overnight to obtain recombinant variants.

Biosynthesis of SAM Catalyzed by BfMAT and Its Variants

The reaction was performed based on the previous report [14] with slight modification. The reaction mixture (500 μL) contained 100 mU/mL *Bf*MAT solution, 20 mM $MgCl_2$, 100 mM KCl, 10 mM ATP, 10 mM Met, and 100 mM Tris–HCl Buffer pH 8.0. The reaction was conducted at 30 ℃ and was terminated by 200 μL 20% perchloric acid. One unit of *Bf*MAT activity is defined as the amount of enzyme required to catalyze the production of 1 μmol of SAM per min. The reaction mixtures were subjected to HPLC analysis.

Kinetic Parameter Assays

The kinetic parameters of MAT were determined in 100 mM Tris–HCl (pH 8.0), 20 mM $MgCl_2$, 100 mM KCl, 2 mM L-methionine, and varying amounts of ATP (0.001 − 2 mM). The reaction was performed with 10 μL 100 mU/mL MAT in 500 μL reaction mixture at 37 ℃ for 10 min, and 100 μL 20% (v/v) perchloric acid was added to stop the reaction.

After centrifugation at 12,000 rpm for 10 min, the product SAM was determined by HPLC (Agilent Technologies 1260 infinity).

For HPLC analysis, a Diamonsil C18 column (250 mm × 4.6 mm, 5 μm) as the stationary phase was used. The mobile phase consisted of a mixture of V (50 mM KH_2PO_4, 5 mM sodium pentanesulfonate) and V (methanol) in a ratio of 85:15. The pH of the mobile phase was adjusted to 3.5 to ensure optimal separation. The flow rate was set at 1 $mL \cdot min^{-1}$ to maintain efficient elution of compounds. For each sample, 10 μL was injected into the system, and detection was performed at a wavelength of 210 nm. The column temperature was maintained at 25 °C throughout the analysis to ensure reproducibility and accurate quantification of the target compounds. The mobile phase was 50 mM potassium dihydrogen phosphate (pH was adjusted to 2.5 with phosphoric acid). The peak retention time for SAM was observed at 2.289 min in the chromatographic analysis (Fig. S5). Kinetic parameters were calculated by nonlinear regression using GraphPad Prism.

Structure Modeling and Molecular Docking

Structure model of MAT was constructed by AlphaFold (https://alphafold.ebi.ac.uk/) [18, 19]. AlphaFold produced a per-residue confidence score (pLDDT) between 0 and 100. pLDDT greater than 90 indicates a high degree of structural confidence. Regions below 50 pLDDT could be unstructured in isolation. pLDDT between 50 and 90 indicates that credibility needs to be considered [18, 19]. Molecular docking calculations with ATP as the ligand were accomplished using the CDOCKER module under a default setting within the active site defined by the Binding-Site module. Briefly, receptor proteins were prepared by eliminating all bound water molecules. Hydrogen atoms were added to the protein optimized by a CHARMm force field. Amino acid residues enclosed within a 5 Å radius sphere centered on the active pocket were selected to create protein conformations and refine side chains. The most stable docking pose with the highest score in CDockScore was chosen as the docking model. Pymol was used for protein structure visualization, and Discovery Studio was used for molecular docking.

Molecular Dynamic Simulation

The obtained protein–ligand complex structure of wild-type *Bf*MAT (WT) and variants were subjected to molecular dynamic (MD) simulation using GROMACS 2019.5, with GROMOS96 43A1 combined atomic force field. Parameters and topology of ATP used in this study were generated using PRODRG2 web server [20]. The unit box is defined as a cube. The edge of the box is 1 nm away from the molecular edge. In addition, different numbers of sodium and chloride ions if needed are added according to the system. In the next step, the energy was minimized and then followed by the equilibration with position restraint on the protein molecules for 0.1 ns using NVT and NPT ensembles. Finally, molecular dynamics simulation was performed at a time scale of 50 ns. The molecular dynamics simulation results were plotted and analyzed by Qtgrace and Dulvy tools.

Interaction and Energy Calculation

The intermolecular interactions are divided into van der Waals interaction and Coulomb interaction in GROMACS. van der Waals interactions include short-range Lenard Jones

potential (LJ) and long-range dispersion interaction. Coulomb interactions include short-range Coulomb interaction and long-range Coulomb interaction. In this study, the van der Waals force between proteins and ligands mainly focused on LJ potential energy. Coulomb interaction is generally considered as long-range interaction, and Particle-mesh Ewald (PME) method is used to deal with the Coulomb interaction in the main body simulation. Short-range and long-range Coulomb interactions are added in the reciprocal space to be the final Coulomb interaction [21]. The energy mentioned above was calculated using the GMX energy module in GROMACS.

Results and Discussion

Gene Mining of MAT Encoding Genes

MAT from *E. coli* (*Ec*MAT) is mostly studied due to its high expression level, easy purification, and resolved crystal structure [14, 22]. However, severe product inhibition of *Ec*MAT limits its applications. To explore more MAT candidates, gene mining was performed with *Ec*MAT as a probe in NCBI (https://www.ncbi.nlm.nih.gov/). According to the sequence alignment (Fig. S1), four MATs sharing 40.0–51.6% sequence identity with *Ec*MAT were selected and expressed in *E. coli* BL21(DE3), including *Campylobacter jejuni* MAT (*Cj*MAT), *Cryptosporidium parvum* MAT (*Cp*MAT), *Thermococcus kodakarensis* MAT (*Tk*MAT), and *Bacteroides fragilis* MAT (*Bf*MAT).

The product inhibition of the above MATs was determined in the presence of 0.1–1 mM SAM. As illustrated in Fig. 1a, the residual activities of all MATs gradually decreased as the increasing SAM concentration. Among them, *Cj*MAT and *Bf*MAT showed better product tolerance. At 1 mM SAM, residual activities of *Cj*MAT and *Bf*MAT were 95.3% and 82.3%, while those of *Ec*MAT and *Tk*MAT were merely 47.8% and 43.6%, respectively. The specific activities of these MATs were also investigated. As shown in Fig. 1b, *Ec*MAT exhibited the highest specific activity (1.89 U/mg) and *Cj*MAT had the lowest activity

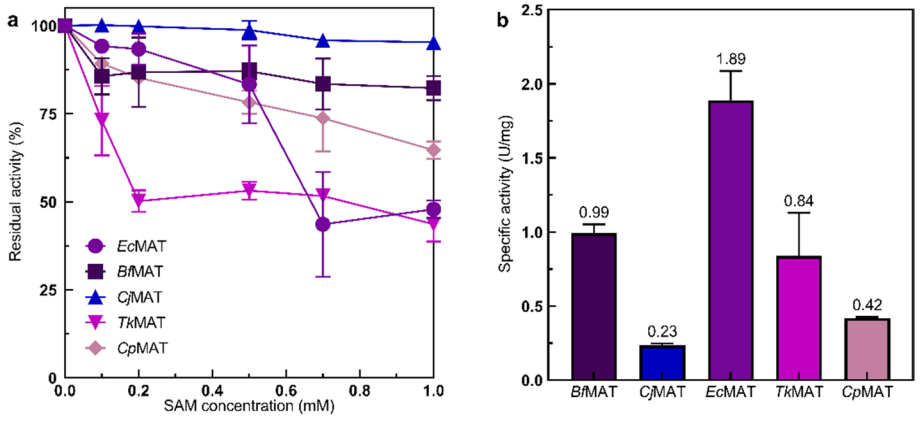

Fig. 1 Product inhibition (**a**) and specific activity (**b**) of MATs from various microorganisms. Reactions were performed using the same amount of WT and variants (100 mU/ mL) at 5 mM MET and 5 mM ATP. For production inhibition experiments, 0–1 mM SAM was added. The activity of reaction without SAM was defined as 100% for the relative activity

(0.23 U/mg). *Bf*MAT and *Tk*MAT showed around half activity of *Ec*MAT. Notably, the specific activity of *Bf*MAT was nearly 4 times higher than that of *Cj*MAT. Therefore, considering its lower product inhibition and moderate specific activity, *Bf*MAT was chosen for further investigations.

Structure Modeling and Semi-rational Engineering of BfMAT

Three-dimensional structures of proteins can provide molecular insights into their catalytic mechanism [23]. Herein, AlphaFold was employed to construct the structure model and guide the modification of *Bf*MAT. The reliability of the predicted structure was evaluated by pLDDT score. As shown in Fig. S2, only one residue Gly105 gave a score of 66.66, and 94.1% of residues received high scores (pLDDT > 90), indicating the high confidence of the structural model of *Bf*MAT constructed by AlphaFold [24], which was used for molecular docking. Considering that ATP is significantly larger than Met and negatively charged, engineering of ATP binding pocket could be critical for the enzymatic activity of *Bf*MAT. As shown in Fig. 2, 16 residues (Val39, Ala40, Glu42, Glu55, Gln98, Ile102, Asp118, Thr267, Gly268, Ile271, Gly284, Gly285, Ala286, Lys290, Lys294, Asp296) within 5 Å around ATP were selected, among which 3 residues (Glu42, Glu55, Lys290) displayed electrostatic interactions with ATP and 2 residues (Ala40 and Ile102) showed Pi-alkyl interactions with ATP.

Saturation mutagenesis of the above-mentioned sites was performed, and the libraries were screened by the high-throughput screening (HTS) method. Five variants showed significantly improved specific activities. As shown in Fig. 3, the specific activities of single variants E42M, E42R, E42C, E55L, and K290I were increased by 37.2%, 25.6%, 34.9%, 18.6%, and 19.8% compared with that of WT (0.86 U/mg). Based on the docking results (Fig. 2), electrostatic interactions between residues E42, E55, and K290 and ATP were observed in WT. When residues E42, E55, and K290 were substituted with uncharged amino acids (e.g., Met, Cys, Leu, and Ile) and positively charged amino acid Arg, their catalytic activities were significantly increased, indicating that modification of electrostatic interactions in ATP binding pocket may contribute to the enhanced activity.

Combinatorial mutagenesis of the above single mutations was performed. All double variants harboring E55L, including E42M/E55L, E42R/E55L, E42C/E55L, and E55L/

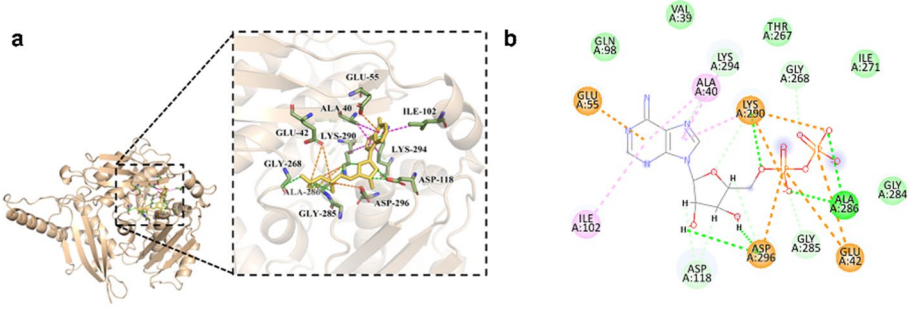

Fig. 2 Molecular docking of *Bf*MAT with ATP. **a** Three-dimensional views of the interactions between key residues and ATP. **b** Two-dimensional views of the interactions between key residues and ATP. Hydrogen bonds: green dashed lines; attractive electrostatic interactions: orange dashed lines; Pi-alkyl interactions: purple dashed lines

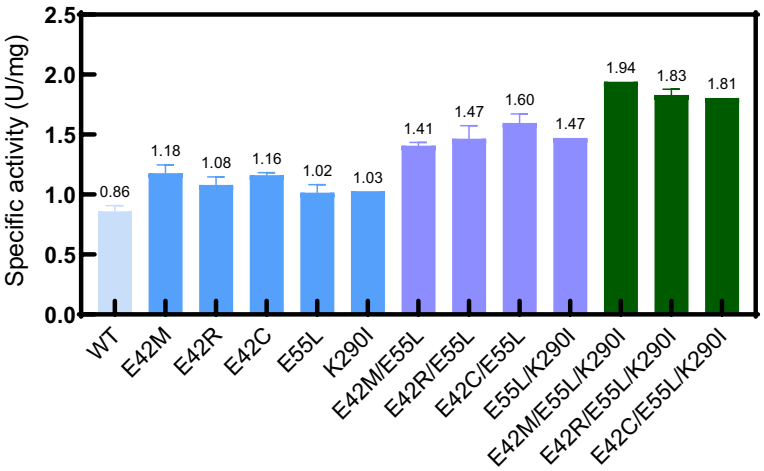

Fig. 3 Specific activities of *Bf*MAT WT and variants of reaction mixture. The mixture (0.5 mL) containing 100 U/mL of purified enzymes, 10 mM ATP, and Met in Tris–HCl buffer (pH 7.5 or 8.0) was incubated at 37 ℃ for 10 min at 120 rpm. The reaction was terminated by adding 200 µL 20% perchloric acid

K290I showed 63.9–86.0% increased activities, suggesting E55L might have synergistic effects with E42M, E42R, E42C, and K290I, whereas variants E42M/K290I, E42R/K290I, and E42C/K290I showed no detectable activity. Subsequently, triple variants M3-1 (E42M/E55L/K290I), M3-2 (E42R/E55L/K290I), and M3-3 (E42C/E55L/K290I) were constructed, and their specific activities were 110.5–125.6% higher than that of that of WT, respectively (Fig. 3). These three triple variants were subjected to further characterization and computational study to understand the mechanism of improved activity.

Enzymatic Characterization of BfMAT and Its Variants

Kinetic Parameters

Kinetic parameters of *Bf*MAT and its variants were determined at varying ATP concentrations (0.001–2 mM) and 2 mM Met. Kinetic parameters of single, double, and triple mutants were listed in Table 1. Compared with WT, E42M and E42C displayed the similar K_m value, but their k_{cat}/K_m values were increased by 62.6% and 58.4%, indicating similar substrate binding capacity and enhanced catalytic efficiency. The K_m values of E55L, E42R, and K290I were 55.6%, 71.6%, and 67.2% higher than that of WT, suggesting reduced substrate affinity. Their k_{cat}/K_m values are similar to that of WT. The K_m value of double variant E42R/E55L was 17.5% lower than that of WT, and its k_{cat}/K_m value was 127.1% higher than that of WT, suggesting the synergistic effect of E42R and E55L on enhanced substrate affinity and catalytic efficiency. There is no significant change in K_m values of E42C/E55L and E55L/K290I, while E42M/E55L displayed a 54.8% increase in K_m value.

The k_{cat}/K_m values of triple mutants M3-1, M3-2, and M3-3 were 4.22, 1.88, and 7.81 times that of WT, respectively. Overall, the lowest K_m value of 11.11 µM was determined with M3-3, which is 60.6% lower than that of WT (28.21 µM), indicating

Table 1 Kinetic parameters of *Bf*MAT WT and variants

	K_m (μM)	k_{cat} (s^{-1})	k_{cat}/K_m ($s^{-1}{\cdot}mM^{-1}$)
WT	28.21	0.79	28.00
E42M	31.70	1.38	43.53
E42R	48.41	1.47	30.37
E42C	29.98	1.33	44.36
E55L	43.90	1.22	27.79
K290I	47.17	1.51	32.01
E42M/E55L	43.68	1.45	33.20
E42R/E55L	23.27	1.48	63.60
E42C/E55L	27.44	1.52	55.39
E55L/K290I	27.29	1.60	58.63
E42M/E55L/K290I	19.36	2.29	118.29
E42R/E55L/K290I	43.03	2.26	52.52
E42C/E55L/K290I	11.11	2.43	218.72

E42M/K290I, E42R/K290I, and E42C/K290I are not included since no activity was detected. The Michaelis–Menten equation curve for the WT is depicted in Fig. S6

its stronger binding capacity with ATP. M3-3 has the highest k_{cat}/K_m value of mutants (218.72 $s^{-1}{\cdot}mM^{-1}$), which is 7.81-fold of WT (28.00 $s^{-1}{\cdot}mM^{-1}$). Compared with WT, the k_{cat}/K_m value of M3-2 was increased by 1.88-fold due to its enhanced k_{cat} value, although its K_m value was 52.5% higher than that of WT. The K_m and k_{cat}/K_m values of M3-1 were 19.36 μM and 118.29 $s^{-1}{\cdot}mM^{-1}$, which was 31.4% lower and 3.22-fold higher than those of WT, respectively.

Optimal pH and Temperature

Influences of pH on *Bf*MAT and its triple variants (M3-1, M3-2, and M3-3) were further investigated. As shown in Fig. 4a, the optimal pH of WT was 8.0, and the activity remained stable (> 90% relative activity) over the range of pH 7.5–8.0. However, its activity dramatically decreased when pH was below 7.5 or above 8.0. Compared with WT, the optimal pH of the triple variants shifted from 8.0 to 7.5. Within the range of pH 8.0–9.0, variants

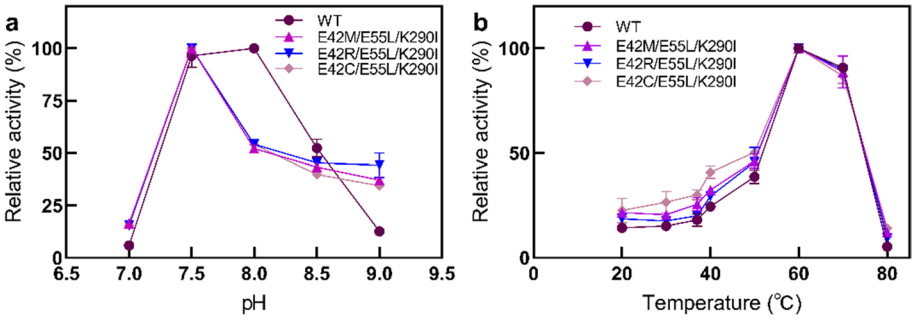

Fig. 4 Optimal reaction pH (**a**) and temperature (**b**) of *Bf*MAT WT and variants. Tris–HCl buffers (0.1 M) of pH 7.0, 7.5, 8.0, 8.5, and 9.0 were used. The highest activity was defined as 100% for the relative activity

displayed relative activities of 40–50%. The change of the optimal pH of variants may be attribute to the decreased electrostatic interactions between ATP and residues (E42, E55, and K290), which may affect the polarity of *Bf*MAT.

Effects of reaction temperature on activities of *Bf*MAT and its triple variants were also investigated. As shown in Fig. 4b, both WT and the variants displayed the same optimal temperature of 60 ℃, as well as similar relative activity profile over 20–80 ℃. With the increase of temperature, the activities of *Bf*MAT and variants gradually increased to the maximum at 60 ℃ and then began to decline. It indicates that mutations have little effect on the optimum reaction temperature of *Bf*MAT.

Product Inhibition

Apart from catalytic activity, product inhibition of MAT is also an important limitation factor for SAM production. The product tolerance of three triple variants was investigated in the presence of varying SAM concentrations (0–1 mM). As showed in Fig. 5, M3-1 exhibited better product tolerance than WT, while variants M3-2 and M3-3 showed slightly higher product inhibition than WT. At 1 mM SAM, M3-1 and WT retained over 80% residual activities, and M3-2 and M3-3 only remained less than 70%. Consequently, variant M3-1 has both enhanced activity and lower product inhibition than WT.

Mechanism of Enhanced Catalytic Performance of BfMAT Variants

Interaction Analysis

MAT-catalyzed reaction is initiated by the sulfur atom of Met, which attacks the carbanion of the adenosine group in ATP (Fig. S3). However, electrostatic interactions near the substrate pocket can potentially hinder the attack of sulfur-positive ion, suggesting that

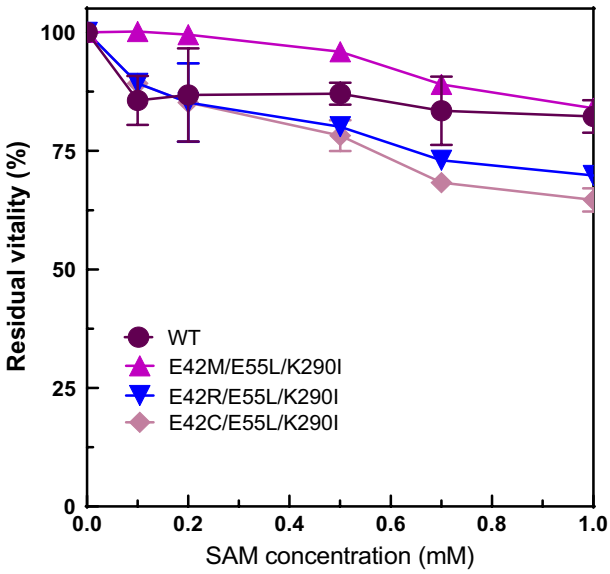

Fig. 5 Product inhibition of *Bf*MAT WT and variants. SAM (0–1 mM) was added to investigate the product tolerance. The activity of WT was defined as 100% for the relative activity

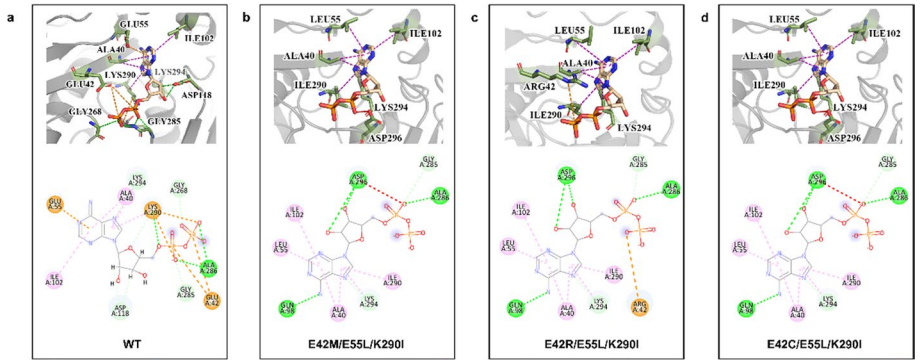

Fig. 6 Interactions between ATP and residues around binding pocket of *Bf*MAT WT and variants. **a** Interactions of WT with ATP. **b** Interactions of E42M/E55L/K290I with ATP. **c** Interactions of E42R/E55L/K290I with ATP. **d** Interactions of E42C/E55L/K290I with ATP. Residues are shown as stick models. Hydrogen bonds: green dashed lines; attractive electrostatic interactions: orange dashed lines; Pi-alkyl interactions: purple dashed lines

Table 2 Energy analysis of *Bf*MAT WT and variants toward ATP

	Lennard–Jones interaction energy(kJ/mol)	Coulomb interaction energy(kJ/mol)	Binding free energy(kJ/mol)
WT	− 157.94	− 17.75	− 83.66
E42M/E55L/K290I	− 185.26	− 5.16	− 94.98
E42R/E55L/K290I	− 192.31	− 17.67	− 87.59
E42C/E55L/K290I	− 187.47	25.76	− 92.73

electrostatic interactions may not be conducive to the reaction. To further investigate the mechanism for enhanced catalytic performance, molecular dockings of the triple variants (M3-1, M3-2, and M3-3) with ATP were performed, and the interactions were analyzed. Five electrostatic interactions between ATP and residues E42, E55, and K290 were observed for WT (Fig. 6a). However, these electrostatic interactions disappeared in variants M3-1 (Fig. 6b) and M3-3 (Fig. 6d). Only one electrostatic interaction was retained in M3-2 due to the introduction of a positively charged amino acid Arg at 42 (Fig. 6c). The attenuated electrostatic interactions between ATP and the variants could be favorable for ATP binding, and thus lead to enhanced catalytic efficiency. Consistent with the electrostatic interaction analysis, variant M3-2 exhibited a higher K_m value compared with WT (Table 1).

MD Simulation and Energy Analysis

MD simulations of WT and triple variants (Fig. S4) were conducted to quantify the energy change of *Bf*MAT-ATP complex. Coulombic interaction is calculated based on the Schrödinger equation that the forces operating within molecules and molecular complexes, which necessarily entails electrostatics [25]. As shown in Table 2, the coulomb interaction energy of M3-1, M3-2, and M3-3 with ATP were − 5.16, − 17.67, and 25.76 kJ/mol,

which were higher than that of WT (− 17.75 kJ/mol), indicating the electrostatic interaction between ATP and substrate pocket is gradually weakening in the variants. In WT, the electronegativity of glutamate at sites 42 and 55 may hinder the contact between Met and ATP in the substrate binding pocket, and thus is unfavorable for the nucleophilic attacks between Met and ATP. Moreover, substitutions of Glu with Met, Arg, Cys, and Lue could decrease the effect of electrostatic interaction, leading to significantly enhanced activity.

Besides, the Lennard–Jones interaction energy of M3-1 (− 185.26 kJ/mol), M3-2 (− 192.31 kJ/mol), and M3-3 (− 187.47 kJ/mol) with ATP are lower than that of WT (− 157.94 kJ/mol), indicating that intermolecular van der Waals is beneficial for substrate binding, while electrostatic interaction is not. In addition, binding free energy is an important parameter in computational biophysics [26]. The binding free energy of WT with ATP (− 83.66 kJ/mol) is higher than that of M3-1 (− 94.98 kJ/mol), M3-2 (− 87.59 kJ/mol), and M3-3 (− 92.73 kJ/mol), revealing that complexes of variants with ATP are more stable than WT (Table 2). Above results show that modification of electrostatic interactions of substrate binding pocket can effectively improve the substrate affinity and catalytic performance of *Bf*MAT.

Conclusion

Semi-rationally engineering was performed to enhance the catalytic activity of *Bf*MAT. The triple variants (M3-1, M3-2, and M3-3) with over 2 times increased specific activity were obtained. Variants M3-1 and M3-3 showed 3.22 and 6.81 folds higher k_{cat}/K_m values than WT, indicating enhanced catalytic efficiency. Based on structural analysis, enhanced catalytic efficiency may be attributed to the attenuated electrostatic interactions between ATP and three key residues (E42, E55, and K290) in variants. MD simulation analysis reveals that the variants exhibit increased coulomb energy and decreased binding free energy compared with WT, providing further evidence for the critical role of electrostatic interactions in catalytic activity of *Bf*MAT. This study demonstrates the significant effect of electrostatic interactions on catalytic performance of *Bf*MAT and provides a potential protein engineering strategy for MATs and related enzymes.

Supplementary Information The online version contains supplementary material available at https://doi.org/10.1007/s12010-023-04676-7.

Author Contribution All authors contributed to the study conception and design. Material preparation was performed by Jinghui Zhou and Gang Xu; data collection and analysis were performed by Weibin Lin, Qiangqiang Wang, Ruizhi Han, and Ye Ni. Funding acquisition was performed by Ruizhi Han and Ye Ni. The first draft of the manuscript was written by Weibin Lin, and all authors commented on previous versions of the manuscript. All authors read and approved the final manuscript.

Funding This work was supported by National Key Research and Development Program (2021YFC2102700), National Natural Science Foundation of China (31871738, 22077054, 21776112), National First-Class Discipline Program of Light Industry Technology and Engineering (LITE2018-07), Program of Introducing Talents of Discipline to Universities (111–2-06) for the financial support of this research. Authors Jinghui Zhou and Gang Xu have received research support from Hunan Flag Bio-tech Co., Ltd.

Data Availability All data have been provided in the manuscript and experimentary material.

Declarations

Ethics Approval Not applicable.

Consent to Participate Informed consent was obtained from all individual participants included in the study.

Consent for Publication All authors have their consent to publish their work.

Competing Interests The authors declare no competing interests.

References

1. Hardy, M. L., Coulter, I., Morton, S. C., Favreau, J., Venuturupalli, S., Chiappelli, F., Rossi, F., Orshansky, G., Jungvig, L. K., Roth, E. A., Suttorp, M. J., & Shekelle, P. (2003). S-adenosyl-L-methionine for treatment of depression, osteoarthritis, and liver disease. *Evidence Report/Technology Assessment, 64*, 1–3.
2. Zano, S. P., Bhansali, P., Luniwal, A., & Viola, R. E. (2013). Alternative substrates selective for S-adenosylmethionine synthetases from pathogenic bacteria. *Archives of Biochemistry and Biophysics, 536*, 64–71.
3. Miller, S. A., & Bandarian, V. (2019). Analysis of electrochemical properties of S-adenosyl-l-methionine and implications for its role in radical SAM enzymes. *Journal of the American Chemical Society, 141*, 11019–11026.
4. Mato, J. M., & Lu, S. C. (2007). Role of S-adenosyl-L-methionine in liver health and injury. *Hepatology, 45*, 1306–1312.
5. Galizia, I., Oldani, L., Macritchie, K., Amari, E., Dougall, D., Jones, T. N., Lam, R. W., Massei, G. J., Yatham, L. N., & Young, A. H. (2016). S-adenosyl methionine (SAMe) for depression in adults. *Cochrane Database of Systematic Reviews, 10*, CD011286.
6. Hosea Blewett, H. J. (2008). Exploring the mechanisms behind S-adenosylmethionine (SAMe) in the treatment of osteoarthritis. *Critical Reviews in Food Science and Nutrition, 48*, 458–463.
7. Katyal, J., Kumar, H., Joshi, D., & Gupta, Y. K. (2017). S-adenosyl methionine (SAM) attenuates the development of tolerance to analgesic activity of morphine in rats. *Neuroscience Letters, 645*, 67–73.
8. Chu, J., Qian, J., Zhuang, Y., Zhang, S., & Li, Y. (2013). Progress in the research of S-adenosyl-L-methionine production. *Applied Microbiology and Biotechnology, 97*, 41–49.
9. Cai, D., Zhang, B., Zhu, J., Xu, H., Liu, P., Wang, Z., Li, J., Yang, Z., Ma, X., & Chen, S. (2020). Enhanced bacitracin production by systematically engineering S-adenosylmethionine supply modules in *Bacillus licheniformis*. *Frontiers in Bioengineering and Biotechnology, 8*, 305.
10. Chen, H., Chu, J., Zhang, S., Zhuang, Y., Qian, J., Wang, Y., & Hu, X. (2007). Intracellular expression of Vitreoscilla hemoglobin improves S-adenosylmethionine production in a recombinant *Pichia pastoris*. *Applied Microbiology and Biotechnology, 74*, 1205–1212.
11. Hu, X., Chu, J., Zhang, S., & Zhuang, Y. (2014). Comparative performance of S-adenosyl-L-methionine biosynthesis and degradation in Pichia pastoris using different promoters and novel consumption inhibitors. *Enyzme and Microbial Technology, 55*, 94–99.
12. Liu, W., Tang, D., Shi, R., Lian, J., Huang, L., Cai, J., & Xu, Z. (2019). Efficient production of S-adenosyl-l-methionine from dl-methionine in metabolic engineered Saccharomyces cerevisiae. *Biotechnology and Bioengineering, 116*, 3312–3323.
13. Park, J., Tai, J., Roessner, C. A., & Scott, A. I. (1996). Enzymatic synthesis of S-adenosyl-l-methionine on the preparative scale. *Bioorganic & Medicinal Chemistry, 4*, 2179–2185.
14. Wang, X., Jiang, Y., Wu, M., Zhu, L., Yang, L., & Lin, J. (2019). Semi-rationally engineered variants of S-adenosylmethionine synthetase from Escherichia coli with reduced product inhibition and improved catalytic activity. *Enyzme and Microbial Technology, 129*, 109355.
15. Dippe, M., Brandt, W., Rost, H., Porzel, A., Schmidt, J., & Wessjohann, L. A. (2015). Rationally engineered variants of S-adenosylmethionine (SAM) synthase: Reduced product inhibition and synthesis of artificial cofactor homologues. *Chemical Communications (Cambridge, England), 51*, 3637–3640.
16. Zheng, H., Yang, S.-J., Zheng, Y.-C., Cui, Y., Zhang, Z., Zhong, J.-Y., & Zhou, J. (2020). Electrostatic effect of functional surfaces on the activity of adsorbed enzymes: Simulations and experiments. *ACS Applied Materials & Interfaces, 12*, 35676–35687.

17. Yunus, I. S., Palma, A., Trudeau, D. L., Tawfik, D. S., & Jones, P. R. (2020). Methanol-free biosynthesis of fatty acid methyl ester (FAME) in Synechocystis sp. PCC 6803. *Metabolic Engineering, 57*, 217–227.
18. Varadi, M., Anyango, S., Deshpande, M., Nair, S., Natassia, C., Yordanova, G., Yuan, D., Stroe, O., Wood, G., Laydon, A., Žídek, A., Green, T., Tunyasuvunakool, K., Petersen, S., Jumper, J., Clancy, E., Green, R., Vora, A., Lutfi, M., … Velankar, S. (2021). AlphaFold Protein Structure Database: Massively expanding the structural coverage of protein-sequence space with high-accuracy models. *Nucleic Acids Res, 50*, 439–444.
19. Jumper, J., Evans, R., Pritzel, A., Green, T., Figurnov, M., Ronneberger, O., Tunyasuvunakool, K., Bates, R., Žídek, A., Potapenko, A., Bridgland, A., Meyer, C., Kohl, S. A. A., Ballard, A. J., Cowie, A., Romera-Paredes, B., Nikolov, S., Jain, R., Adler, J., … Hassabis, D. (2021). Highly accurate protein structure prediction with AlphaFold. *Nature, 596*, 583–589.
20. Schüttelkopf, A. W., & van Aalten, D. M. F. (2004). PRODRG: A tool for high-throughput crystallography of protein-ligand complexes. *Acta Crystallographica. Section D Biological Crystallography, 60*, 1355–1363.
21. Brief notes on analysis of molecular dynamics simulation results of GROMACS protein ligand 2021. Available from: https://zhuanlan.zhihu.com/p/149863158. Accessed 14 Oct 2021.
22. Michailidou, F., Klöcker, N., Cornelissen, N. V., Singh, R. K., Peters, A., Ovcharenko, A., Kümmel, D., & Rentmeister, A. (2021). Engineered SAM synthetases for enzymatic generation of AdoMet analogs with photocaging groups and reversible DNA modification in cascade reactions. *Angewandte Chemie, 60*, 480–485.
23. Waterhouse, A., Bertoni, M., Bienert, S., Studer, G., Tauriello, G., Gumienny, R., Heer, F. T., de Beer, T. A. P., Rempfer, C., Bordoli, L., Lepore, R., & Schwede, T. (2018). SWISS-MODEL: Homology modelling of protein structures and complexes. *Nucleic Acids Research, 46*, W296–W303.
24. Varadi, M., Anyango, S., Deshpande, M., Nair, S., Natassia, C., Yordanova, G., Yuan, D., Stroe, O., Wood, G., Laydon, A., Žídek, A., Green, T., Tunyasuvunakool, K., Petersen, S., Jumper, J., Clancy, E., Green, R., Vora, A., Lutfi, M., … Velankar, S. (2022). AlphaFold Protein Structure Database: Massively expanding the structural coverage of protein-sequence space with high-accuracy models. *Nucleic Acids Research, 50*, D439–D444.
25. Politzer, P., Murray, J. S., & Clark, T. (2021). The π-hole revisited. *Physical Chemistry Chemical Physics, 23*, 16458–16468.
26. Wang, L., Chambers, J., & Abel, R. (2019). Protein-ligand binding free energy calculations with FEP. *Methods in Molecular Biology, 2022*, 201–232.